Nanoscale Res Lett (2010) 5:1418–1423
DOI 10.1007/s11671-010-9655-5

NANO EXPRESS

Synthesis and White-Light Emission of ZnO/HfO_2: Eu Nanocables

Lixin Liu · Hongliang Zhang · Yuan Wang · Yurong Su · Ziwei Ma · Yizhu Xie · Haiting Zhao · Changcheng Chen · Yanxia Liu · Xiaosong Guo · Qing Su · Erqing Xie

Received: 7 January 2010 / Accepted: 18 May 2010 / Published online: 1 June 2010

Abstract ZnO/HfO_2:Eu nanocables were prepared by radio frequency sputtering with electrospun ZnO nanofibers as cores. The well-crystallized ZnO/HfO_2:Eu nanocables showed a uniform intact core–shell structure, which consisted of a hexagonal ZnO core and a monoclinic HfO_2 shell. The photoluminescence properties of the samples were characterized. A white-light band emission consisted of blue, green, and red emissions was observed in the nanocables. The blue and green emissions can be attributed to the zinc vacancy and oxygen vacancy defects in ZnO/HfO_2:Eu nanocables, and the yellow–red emissions are derived from the inner 4f-shell transitions of corresponding Eu^{3+} ions in HfO_2:Eu shells. Enhanced white-light emission was observed in the nanocables. The enhancement of the emission is ascribed to the structural changes after coaxial synthesis.

Keywords ZnO · HfO_2:Eu · Nanocables · White-light emission · Electrospinning

Introduction

Transition metal oxide HfO_2 activated by RE ions has recently attracted great attention for the luminescent applications, due to its rather large band gap of 5.8 eV, high refractive index, good transparency in visible spectral range and low phonon energies. Recently, a number of papers concerning the photoluminescence of RE ions in HfO_2 have been published [1–3]. It has been demonstrated that doping luminescent RE ions into nano-hosts is an optimistic approach to develop efficient and stable nanophosphors [4–6]. However, there are few reports on the luminescence properties of one-dimensional (1D) HfO_2: RE-based materials, which will have potential applications in white-light nanodevices, such as light-emitting diodes (LEDs) and flat panel displays. As well known, zinc oxide (ZnO) shows a broad-band light emission in the blue–yellow region, and it has been considered to be a potential material for light-emitting devices [7, 8]. During the recent years, the fabrication and characterization of ZnO-based nanoscale materials have received much attention [9]. Many studies have reported that nano-scaled ZnO exhibits a unique luminescent property different from that of the bulk ZnO [10–13]. Because nanostructures possess a much higher surface-to-volume ratio, the interaction between ZnO nanostructures and surrounding materials can strongly affect the emission spectra and thus offers an effective approach to urge its optoelectronic properties. Thus, it is worth investigating the PL properties of ZnO/HfO_2:RE nanostructures.

Many methods have already been demonstrated for generating 1D nanocables [14–17]. Electrospinning and sputtering together could provide a simple synthetic technique for preparing nanocables. Electrospinning has provided a simple approach to fabricate exceptionally uniform nanofibers with long length, much thin diameter, and diversified composition [18–20]. Several groups have used polyvinylpyrolidone (PVP), polyvinyl alcohol (PVA), and other polymers as electrospun templates to load inorganic precursors [18, 21, 22]. Then, the coating of nanofibers can be easily prepared by sputtering [23].

L. Liu · H. Zhang · Y. Wang · Y. Su · Z. Ma · Y. Xie · H. Zhao · C. Chen · Y. Liu · X. Guo · Q. Su · E. Xie (✉)
Key Laboratory for Magnetism and Magnetic Materials of the Ministry of Education, Lanzhou University, 730000 Lanzhou, People's Republic of China
e-mail: xieeq@lzu.edu.cn

In this work, we report an approach to efficiently fabricate ZnO/HfO_2:Eu nanocables by sputtering Eu-doped HfO_2 shells onto electrospun ZnO nanofiber cores. ZnO nanofibers were prepared by annealing of the electrospun fibers of PVA/zinc acetate composite. Then, the PL spectrum of the sample annealed at 700°C was investigated. The ZnO/HfO_2:Eu nanocables show intense white emission with broad visible bands covering from blue to red range. This method is also suitable for the synthesis of other nanocable materials.

Experimental Details

Preparation of ZnO Nanofiber Cores

ZnO nanofibers were prepared by calcination of the electrospun fibers of PVA/zinc acetate composite. The experiments were carried out as the following procedures: First, 0.25 g PVA (Sigma–Aldrich, Mw $\approx$ 80,000), 0.5 g zinc acetate ($Zn(CH_3COO)_2\cdots 2H_2O$), and 0.059 g glacial acetic acid (CH_3COOH) were dissolved into 2 ml deionized water followed by vigorous magnetic stirring in a water bath at 60°C for 3 h. Thus, a viscous gel of PVA/zinc acetate composite solution was obtained. Then, the solution was held in a glass syringe equipped with a stainless needle, whose inner diameter is about 0.5 mm. This needle simultaneously served as an electrode and was connected to the anode of a DC high-voltage source. During the electrospinning process, the distance and the applied voltage between the needle and the collectors were 17 cm and 25 kV, respectively. The electrospun fibers were collected on the n-type (111) silicon substrates. Finally, the as-prepared samples were annealed at 600°C for 2 h in O_2 ambient to remove the PVA and make the zinc acetate decomposing to ZnO compositions.

Deposition of HfO_2 Shells

HfO_2 shells were prepared by RF reactive magnetron sputtering onto the ZnO nanofibers collected on Si substrates. Prior to deposition, the sputtering chamber was pumped down to 10^{-4} Pa by a turbomolecular pump. A 4-inch hafnium target (99.95%) with a target–substrate distance of 50 mm was used, and pieces of Eu_2O_3 (area ratio of Eu_2O_3/Hf is about 3%) were placed on the target to sputter HfO_2:Eu shells. The ratio of argon (99.99%) to oxygen (99.99%) (Ar/O_2) was kept at 2.12 during the sputtering. The deposition pressure and sputtering power were maintained at 0.2 Pa and 200 W, respectively. Ultimately, the as-prepared samples were annealed at 700°C for 2 h in O_2 ambient to crystallize the ZnO/HfO_2 nanocables and make Eu ions activated.

For comparison, HfO_2:Eu nanotubes were also prepared at the same sputtering parameters on the PVP-nanofiber templates, which were prepared with the PVP/ethanol solution by electrospinning. Then the sample was annealed at 700°C in O_2 ambient resulting in HfO_2:Eu nanotubes.

Characterization

The morphologies of the ZnO/HfO_2 nanocables were characterized by field emission scanning electron microscope (FESEM, Hitachi S-4800, operated at 5 kV) and high-resolution transmission electron microscope (HRTEM, FEI Tecnai F30, operated at 300 kV). The crystalline structure was examined by XRD and Raman spectroscopy. The XRD experiments were performed on a Philips X' Pert diffractometer with Cu Kα1 radiation ($\lambda = 1.54056$ Å) by glancing incidence in the θ–2θ configuration. Raman spectroscopy was performed in a backscattering geometry using a micro-Raman system (Jobin–Yvon, J. Y. HR 800), a 325 nm line (3.82 eV) of a 15 mW He–Cd laser was used as the excitation source. The PL spectra were recorded on a spectrophotometer (SHI-MADZU, RF-540) using a 15 mW He–Cd laser with a wavelength of 325 nm as the excitation source.

Results and Discussion

The typical morphologies of the samples can be observed from the SEM images. Figure 1a shows the general morphology of the ZnO/HfO_2 coaxial nanocables, indicating that the nanocables annealed at 700°C are uniform and smooth. The cross-section of a typical nanocable (inset of Fig. 1a) shows that the nanocables have an intact core–shell structure with an average outer diameter of about 200 nm. Figure 1b shows the ZnO nanofibers annealed at 600°C without sputtered HfO_2 shells, the nanofibers are uniform and standing free with an average diameter of 100 nm (inset of Fig. 1b). Such uniform cores lead to the growth of the high-degree coaxial nanocables. Moreover, the chemical composition of the ZnO/HfO_2 nanocables analyzed by the energy dispersive spectrometry (EDS) indicates that there are Hf, Zn, and O elements in the cables, as shown in Fig. 1c.

Further studies have been investigated by TEM. Figure 2 displays a typical TEM image of the annealed ZnO/HfO_2 nanocables. It can be seen that the ZnO/HfO_2 nanocables possess a coaxial structure, that is, a thin sheath with lighter contrast is formed outside the surface of nanofiber-like structure of dark contrast. The dark contrast can be attributed to a thick and different material at the core, indicating that the cables have a uniform core–shell structure with a sheath thickness of about 50 nm, and a

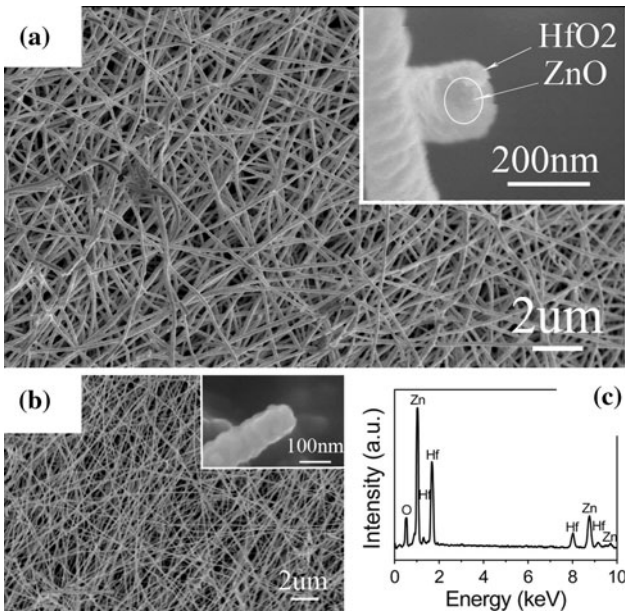

Fig. 1 **a** SEM images of the ZnO/HfO_2:Eu nanocables annealed at 700°C. The inset in **a** is the cross-section image of a nanocable. **b** SEM images of the ZnO nanofibers annealed at 600°C. **c** The EDS pattern of the nanocables, suggesting that the nanocables contain Hf, Zn, and O

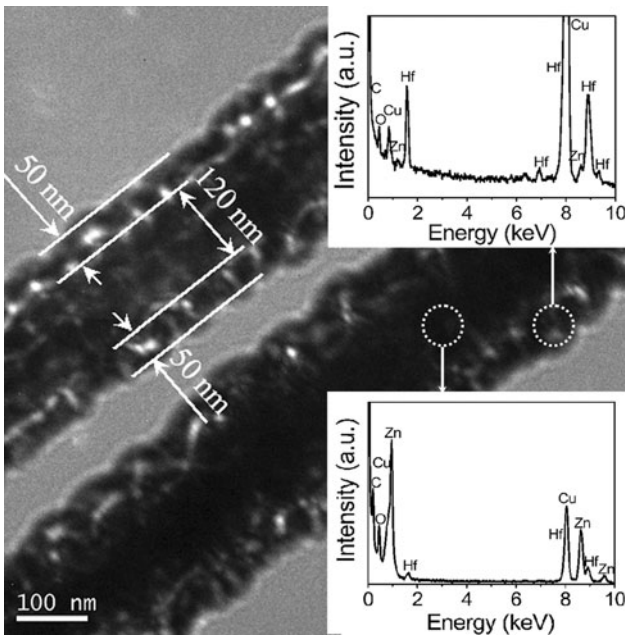

Fig. 2 Typical TEM image of the ZnO/HfO_2:Eu nanocables annealed at 700°C. The insets are the EDS taken from the cable center and the shell, respectively, indicating that the nanocables contain Hf, Zn, and O, the shells contain Hf and O only (a little number of Zn can be ascribed to the interface of ZnO and HfO_2)

core diameter of about 120 nm. These results agree with our SEM analysis. Additionally, the insets of the Fig. 2 show that the EDS patterns detected from different areas of the coaxial structure, as directed by the arrows. It can be seen that the coaxial cable is mainly composed of Zn, Hf, and O elements, while the shell layer only consists of Hf and O (a little number of Zn can be attributed to the interface of ZnO and HfO_2). The Cu and C signals should be ascribed to the copper grid coated with porous carbon film for supporting sample.

The existence of ZnO and HfO_2 in the nanocables is also confirmed by XRD and Raman spectra. Figure 3 shows XRD pattern of the coaxial nanocables annealed at 700°C. The peak positions are well consistent with those of hexagonal ZnO (JCPDS No. 80-0075) and monoclinic HfO_2 (JCPDS No. 78-0050). In the pattern, the peaks at 31.71° and 34.40° correspond not only to the (100) and (002) planes of hexagonal ZnO, but also to the (111) and (002) planes of monoclinic HfO_2. Compared with those ZnO peaks, the peaks of HfO_2 are broader and some of them are not clearly observed due to its relative low crystalline quality. The average grain sizes of the nanocables estimated from the peaks of ZnO and HfO_2 by the Scherrer formula are 17.8 and 8.9 nm, respectively.

A typical Raman spectrum of the ZnO/HfO_2:Eu nanocables is shown in Fig. 4. The peaks centered at 430 and 565 cm^{-1} can be assigned to the E_2(high) and A_1(LO) modes of hexagonal ZnO, respectively [24, 25]. Compared

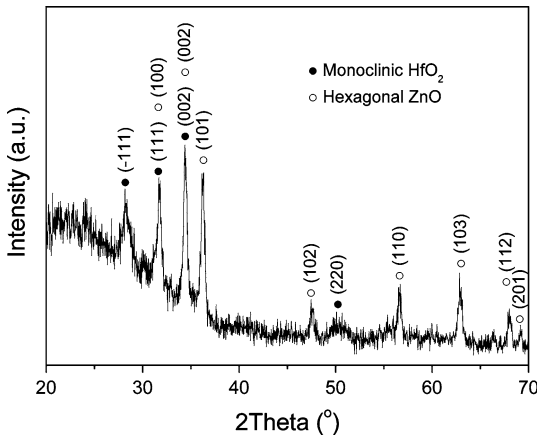

Fig. 3 XRD pattern of HfO_2 ZnO/HfO_2:Eu nanocables annealed at 700°C. Symbols (*filled circle*) and (*open circle*) correspond to monoclinic HfO_2 and hexagonal ZnO, respectively

with reported phonon frequencies of 437 and 574 cm^{-1} of bulk ZnO, the E_2(high) and A_1(LO) peaks redshift by 7 and 9 cm^{-1}, respectively. These redshifts might be ascribed to the phonon localization by defects and impurities, and the laser-induced heating in the ZnO nanocrystals [26]. The peak at 496 cm^{-1} can be assigned to the A_g strongest vibration mode of monoclinic HfO_2 [27, 28]. The broadening of the scattering peaks is probably due to the reduced phonon coherence caused by the finite size of the nanocrystals and the presence of defects in the sample.

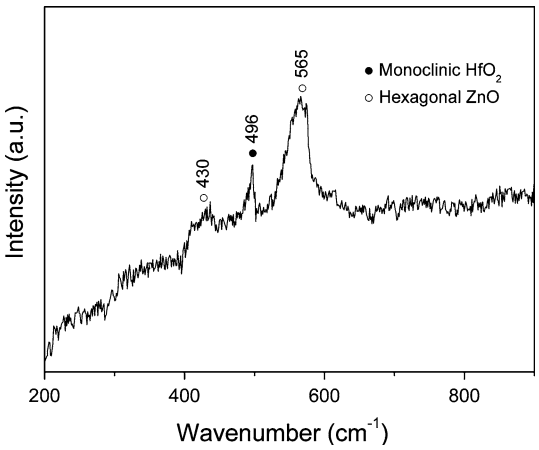

Fig. 4 Raman spectrum of ZnO/HfO_2:Eu nanocables annealed at 700°C. Symbols (*filled circle*) and (*open circle*) correspond to monoclinic HfO_2 and hexagonal ZnO, respectively

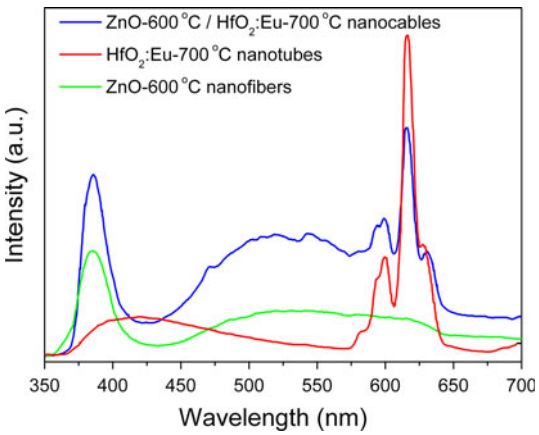

Fig. 5 PL spectra of ZnO nanofibers, HfO_2:Eu nanotubes, and ZnO/HfO_2:Eu nanocables at room temperature using the 325 nm line of a Hd–Cd laser as the excitation source

Figure 5 shows PL spectra of ZnO nanofibers, HfO_2:Eu nanotubes, and ZnO/HfO_2:Eu nanocables annealed at 600 and 700°C, respectively. It can be seen that the emission bands of the ZnO/HfO_2:Eu nanocables consist of that of ZnO nanofibers and HfO_2:Eu nanotubes, and white-light emission is observed from the nanocables. The near-band-edge emission peak at 384 nm in the ultraviolet region may originate from the exciton recombination through an exciton–exciton collision process in ZnO [7]. The blue and green–yellow emission can be mainly ascribed to the defect-related deep-level emission of ZnO cores, and the yellow–red emission is derived from the Eu-doped HfO_2 shells, as shown in the spectra. These emission bands of the ZnO/HfO_2:Eu nanocables originate from the combined action of the ZnO nanocores and Eu-doped HfO_2 shells.

However, for the nanocables, though the positions of the emission bands in the UV to green–yellow region are similar to those of ZnO nanofibers, the intensities of these bands, especially the visible emission bands increase significantly. These show that HfO_2 shells have great effect on the PL properties of ZnO cores. When the HfO_2 shells are coated onto the ZnO nanofibers, the interaction between the interface of ZnO and HfO_2 is strong enough, thus Hf_xZn_yO may be formed at the interface of the heterostructure. The interfacial Hf_xZn_yO is formed by the O, Zn, and Hf atoms diffusion and restructuring at the interface of the nanocables. This diffusion and restructuring would increase more radiative-related defects in the bulk of ZnO, especially oxygen vacancies, leading to the intensity increase of visible region emission of the ZnO cores. The enhanced UV emission mainly results from the reduction of non-radiative recombination centers in the nanocores by higher temperature annealing [29, 30]. Since the ZnO cores were re-annealed in O_2 ambient at a higher temperature of 700°C for 2 h during the post-annealing of the HfO_2 shells, the concentration of non-radiative transition centers could be reduced. Thus, the emission bands in the UV to green–yellow region related to the ZnO cores are enhanced.

In order to further investigate the PL properties of the nanocables, Gaussian fitting was performed to clarify the emission lines. The fitting results of the sample are shown in Fig. 6. The fitting emission bands located at 472, 509, and 555 nm can be mainly attributed to deep-level defects emissions in ZnO cores, and the 509 nm band can be partially ascribed to oxygen vacancies emission in monoclinic HfO_2 [31, 32]. Among those visible emissions in ZnO, the green emissions (509 and 555 nm) can be ascribed to the radiative recombination of electrons from the conduction band edge to the deeply trapped holes level $V_o^{\cdot\cdot}$ [10, 11, 33, 34]. And the blue emission of 472 nm is related to the recombination of electrons from the conduction band edge to V_{zn} [10]. However, some papers reported that the

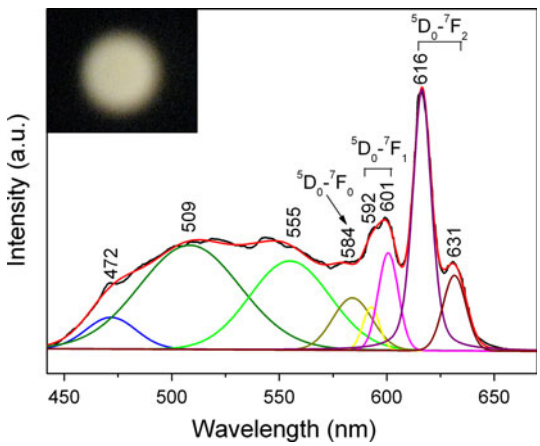

Fig. 6 Gaussian fitting curves of PL spectrum of the ZnO/HfO_2:Eu nanocables. The inset is the luminescence photograph of the nanocables

blue emission can be assigned to the oxygen vacancies or Zn interstitials [35–37], and its mechanism is still in controversy. In this work, the Hf_xZn_yO interfacial layer is formed, which gives rise to V_{Zn}' in the depletion region that is created by the band bending in the heterogeneous boundaries, resulting in the increase of blue emission. Therefore, the defect level responsible for the blue emission can be assigned to V_{Zn}' that is about 0.7 eV above the valence band [10]. Inside of the ZnO nanocores, the recombination centers of oxygen vacancies increase as a result of the formation of Hf_xZn_yO interfacial layer, leading to the enhancement of green emission.

The peaks centered at 584, 592, 601, 616, and 631 nm are assigned to the $^5D_0 \rightarrow {}^7F_0$, $^5D_0 \rightarrow {}^7F_1$, $^5D_0 \rightarrow {}^7F_1$, $^5D_0 \rightarrow {}^7F_2$, and $^5D_0 \rightarrow {}^7F_2$ transitions of Eu^{3+} ions, respectively. These emission peaks are the same as that of HfO_2:Eu^{3+} nanotubes, which cover yellow and red regions of the visible light. The strongest emission peak at 616 nm is responsible for the characteristic red-light emission of $^5D_0 \rightarrow {}^7F_2$ transition. The intensity ratio of the $^5D_0 \rightarrow {}^7F_2$ and $^5D_0 \rightarrow {}^7F_1$ is 2.0, indicating that such spectra are typical emission of Eu^{3+} ions in a monoclinic surrounding [38, 39]. Moreover, the intense light emission could be received in the HfO_2:RE^{3+} nanostructures due to their high density of surface states [40]. As a result, the enhanced blue, green and red bands are emitted simultaneously, and an almost white light is observed. The luminescence spot on the sample is insetted in Fig. 6.

Conclusions

ZnO/HfO_2:Eu nanocables have been prepared by a novel approach that combined electrospinning and sputtering techniques. The well-crystallized nanocables have a uniform intact hexagonal ZnO core/monoclinic HfO_2 shell structure. The PL measurements show that the nanocables emit white light covering from UV to red spectra range. The presence of UV may originate from the exciton recombination in ZnO, the blue and green emissions are attributed to the deep-level defects in ZnO/HfO_2:Eu nanocables, and the yellow–red emissions are derived from the inner 4f-shell transitions of corresponding Eu^{3+} ions in HfO_2:Eu shells. Enhanced white-light emission is achieved from the nanocables, revealing that the ZnO/HfO_2:Eu nanocables are efficient white-light emission material. The interaction between the interface of ZnO and HfO_2 could be responsible for the enhancement of PL property in the blue and green regions. These ZnO/HfO_2:Eu core–shell nanostructures have many potential applications such as white-light nanodevices and nanoscale FET semiconductor devices.

Acknowledgments This work was supported by NSAF Joint Funds of the National Natural Science Foundation of China (Grant No. 10776010).

References

1. S. Lange, V. Kiisk, J. Aarik, M. Kirm, I. Sildos, Phys. Stat. Sol. (c) **4**, 938 (2007)
2. A. Monteil, M. El-Jouad, G. Alombert-Goget, S. Chaussedent, N. Gaumer, A. Mahot, A. Chiasera, Y. Jestin, M. Ferrari, J. Non-Cryst. Solids **354**, 4719 (2008)
3. E. Zych, M. Wojtowicz, A. Dobrowolska, L. Kepinski, Opt. Mater. **31**, 1764 (2009)
4. L. Li, C.K. Tsung, Z. Yang, G.D. Stucky, L. Sun, J. Wang, C. Yan, Adv. Mater. **20**, 903 (2008)
5. E. Nogales, B. M′endez, J. Piqueras, J.A. Garc′ıa, Nanotechnology **20**, 115201 (2009)
6. M.K. Devaraju, S. Yin, T. Sato, Nanotechnology **20**, 305302 (2009)
7. J.G. Ma, Y.C. Liu, C.S. Xu, Y.X. Liu, C.L. Shao, H.Y. Xu, J.Y. Zhang, Y.M. Lu, D.Z. Shen, X.W. Fan, J. Appl. Phys. **97**, 103509 (2005)
8. J.H. Choy, E.S. Jang, J.H. Won, J.H. Chung, D.J. Jang, Y.W. Kim, Adv. Mater. **15**, 1911 (2003)
9. H.J. Fan, F. Bertram, A. Dadgar, J. Christen, A. Krost, M. Zacharias, Nanotechnology **15**, 1401 (2004)
10. Y.Y. Peng, T.E. Hsieh, C.H. Hsu, Nanotechnology **17**, 174 (2006)
11. A. Dijken, E.A. Meulenkamp, D. Vanmaekelbergh, A. Meijerink, J. Lumin. **87–89**, 454 (2000)
12. D. Jiang, L. Cao, W. Liu, G. Su, H. Qu, Y. Sun, B. Dong, Nanosc. Res. Lett. **4**, 78 (2009)
13. S. M̈uller, M. Zhou, Q. Li, C. Ronning, Nanotechnology **20**, 125704 (2009)
14. L. Dai, X.L. Chen, X. Zhang, T. Zhou, B. Hu, Appl. Phys. A **78**, 557 (2004)
15. Y. Zhang, K. Suenaga, C. Colliex, S. Iijima, Science **281**, 973 (1998)
16. X. Wang, P. Gao, J. Li, C.J. Summers, Z.L. Wang, Adv. Mater. **14**, 1732 (2002)
17. Q. Wei, W. Zhou, J. Ji, J. Shen, Nanosc. Res. Lett. **4**, 84 (2009)
18. A. Greiner, J.H. Wendorff, Angew. Chem. Int. Ed. **46**, 5670 (2007)
19. D. Li, Y. Xia, Adv. Mater. **16**, 1151 (2004)
20. R.A. Caruso, J.H. Schattka, A. Greiner, Adv. Mater. **13**, 1577 (2001)
21. X.M. Sui, C.L. Shao, Y.C. Liu, Appl. Phys. Lett. **87**, 113115 (2005)
22. D. Li, Y. Wang, Y. Xia, Adv. Mater. **16**, 361 (2004)
23. H.W. Kim, M.A. Kebede, H.S. Kim, Opt. Mater. **31**, 1853 (2009)
24. T.C. Damen, S.P.S. Porto, B. Tell, Phys. Rev. **142**, 570 (1966)
25. X.D. Guo, R.X. Li, Y. Hang, Z.Z. Xu, B.K. Yu, H.L. Ma, X.W. Sun, Mater. Lett. **61**, 4583 (2007)
26. K.A. Alim, V.A. Fonoberov, A.A. Balandin, Appl. Phys. Lett. **86**, 053103 (2005)
27. A. Jayaraman, S.Y. Wang, S.K. Sharma, Phys. B **48**, 9205 (1993)
28. P.E. Quintard, P. Barbe′ris, A.P. Mirgorodsky, T. Merle–Me′jean, J. Am. Ceram. Soc. **85**, 1745 (2002)
29. W.S. Shi, O. Agyeman, C.N. Xu, J. Appl. Phys. **91**, 5640 (2002)

30. I. Ozerov, M. Arab, V.I. Safarov, W. Marine, S. Giorgio, M. Sentis, L. Nanai, Appl. Surf. Sci. **226**, 242 (2004)
31. D.M. Ramo, J.L. Gavartin, A.L. Shluger, Phys. Rev. B **75**, 205336 (2007)
32. V. Kiisk, S. Lange, K. Utt, T. Tatte, H. Mandar, I. Sildos, Phys. B **405**, 758 (2010)
33. H. He, Y. Wang, Y. Zou, J. Phys. D Appl. Phys. **36**, 2972 (2003)
34. R.C. Wang, C.P. Liu, J.L. Huang, S.J. Chen, Appl. Phys. Lett. **86**, 251104 (2005)
35. W. Cheng, P. Wu, X. Zou, T. Xiao, J. Appl. Phys. **100**, 054311 (2006)
36. B. Lin, Z. Fu, Y. Jia, Appl. Phys. Lett. **79**, 943 (2001)
37. Y.G. Wang, S.P. Lau, H.W. Lee, S.F. Yu, B.K. Tay, X.H. Zhang, H.H. Hng, J. Appl. Phys. **94**, 354 (2003)
38. M. Gaft, G. Panczer, R. Reisfeld, I. Shinno, B. Champagnon, G. Boulon, J. Lumin. **87–89**, 1032 (2000)
39. M. Villanueva-Ibañez, C. Le Luyer, C. Dujardin, J. Mugnier, Mater. Sci. Eng. B **105**, 12 (2003)
40. L.X. Liu, Z.W. Ma, Y.Z. Xie, Y.R. Su, H.T. Zhao, M. Zhou, J.Y. Zhou, J. Li, E.Q. Xie, J. Appl. Phys. **107**, 024309 (2010)